Research Article

Journal of RAMAN SPECTROSCOPY

Received: 9 March 2011 Revised: 13 July 2011 Accepted: 13 July 2011 Published online in Wiley Online Library: 20 September 2011

(wileyonlinelibrary.com) DOI 10.1002/jrs.3047

Identification of minerals and organic materials in Middle Eocene ironstones from the Bahariya Depression in the Western Desert of Egypt by means of micro-Raman spectroscopy

Valerian Ciobotă,[a] Walid Salama,[b] Nicolae Tarcea,[a] Petra Rösch,[a] Mourtada El Aref,[b] Reinhard Gaupp[c] and Jürgen Popp[a,d]*

The Middle Eocene ironstones of the Bahariya Depression consist of four iron ore types: manganiferous mud-ironstone, fossiliferous ironstone, stromatolitic ironstone and nummulitic–ooidal–oncoidal ironstone. The upper surfaces of these sequences were subjected to subaerial weathering and a lateritic iron ore type was formed. The chemical composition of these ironstone types was investigated by means of micro-Raman spectroscopy. Various closely related iron-containing and manganese-containing minerals were detected by means of the above-mentioned approach. The high spatial resolution and sensitivity of this method allowed us to identify minerals that could not be detected by other techniques. Well-preserved organic materials were observed in one type of ironstones. Therefore, using Raman spectroscopy, we were able to provide evidence that the formation of some of the investigated rocks was biologically mediated. The application of Raman spectroscopy is considered a powerful technique for the identification of both organic and inorganic substances in the studied iron ore deposits. Copyright © 2011 John Wiley & Sons, Ltd.

Supporting information may be found in the online version of this article.

Keywords: micro-Raman spectroscopy; mud-ironstone; stromatolitic ironstone; fossiliferous ironstone; nummulitic–ooidal–oncoidal ironstone

Introduction

Ironstones are sedimentary rocks with >15 wt% iron, corresponding to 21.4 wt% Fe_2O_3.[1,2] The ironstones may or may not contain >5 vol.% ooids, pisoids, peloids and oncoids. Ooids are spherical or ellipsoidal coated grains ~2 mm in diameter displaying regular concentric laminae surrounding a central core. Grains similar to ooids but >2 mm are known as pisoids. Oncoids are similar to pisoids, but have a biogenic origin and irregular concentric laminae. Peloids are grains of fine-grained material with diameters in the range of ooids to pisoids, but without recognizable internal structure. These coated grains were formed in either continental or marine depositional environments.[1,2] The distribution of the ooidal ironstones was generally abundant during the Early and Middle Eocene period because of the major changes in the paleogeographic position of the shoreline that occurred during the Eocene Epoch.[3,4]

The main ooidal–oncoidal ironstone deposits of Egypt are well represented in the Western Desert of Egypt. They are located in the northeastern part of the Bahariya Depression in three mine areas, i.e. Ghorabi, El Harra and El Gedida. The Middle Eocene ironstones of the Bahariya Depression are subdivided into two sequences: lower and upper. These ironstone sequences consist of four shallow marine iron ore types. The marine ironstone types include black manganiferous mud-ironstone and yellowish-brown stromatolitic ironstone types, which were formed from colloidal suspension in quiet waters in lagoonal–tidal flat environments, and storm-related black fossiliferous ironstone and shallow subtidal–intertidal yellowish-brown nummulitic–ooidal–oncoidal ironstone types, which were formed during agitated water conditions. The upper surfaces of these sequences were subjected to subaerial weathering, along which lateritic iron ores were formed.[1,2,5] A more detailed description of the investigated samples can be found in the supporting information.

For a fundamental understanding of the origin and evolution of planets, detailed information regarding the crust surface is required. Mineralogical analysis of the surface can be performed successfully using Raman spectroscopy; the identification of inorganic and organic minerals and biological compounds being possible because of it.[6–8] Not only solid state materials but also liquids and gases, which could be present as inclusions in crystalline minerals and glasses, can be investigated by means of Raman spectroscopy. The spatial resolution of the technique can be improved by combining the spectrometer with a microscope allowing for a lateral resolution below 1 μm. In addition, the morphology of various minerals at the rock

* *Correspondence to: Jürgen Popp, Institute of Physical Chemistry, Friedrich Schiller University Jena, Germany. E-mail: juergen.popp@uni-jena.de*

a *Institute of Physical Chemistry, Friedrich Schiller University Jena, Germany*

b *Geology Department, Faculty of Science, Cairo University, Egypt*

c *Institute of Earth Sciences, Friedrich Schiller University Jena, Germany*

d *Institute of Photonic Technology, Jena, Germany*

surface can be investigated using Raman spectroscopy. All the above-mentioned properties of the Raman technique make this method a powerful tool for *in situ* planetary studies.

A number of studies have been dedicated to the application of Raman spectroscopy in archaeology and the arts.[6–12] Investigation of pigments used in paintings,[6,7,11] of varnishes and binding media utilized for art conservation[9,10] or discrimination between genuine and fake artifacts and gems[12] are common applications of Raman spectroscopy in this field. Raman spectroscopy alone, or in combination with other techniques, has also been successfully applied to mineral and organic material characterization and identification.[13–27] Determination of the chemical composition of various meteorites[28–30] and rocks derived from the Earth's surface,[14–16,31] discrimination between closely related minerals[17,18] or detection of biosignatures from geological specimens[32,33] are possible by means of Raman spectroscopy.

The aim of this study was to gain more information about the formation of ironstones. Here, we were especially interested in investigating if biotic components were involved in the formation of ooids and oncoids.

Experimental

For Raman measurements, two types of samples were used: (1) rough and (2) polished. No other sample preparation was performed. Point measurements were carried out on both types of samples. In addition, Raman maps of the polished samples were recorded. On the basis of the frequency of detection of various minerals when point measurements were performed, we concluded that some minerals were more abundant than others.

Raman setup

The Raman measurements of the rocks were performed with a commercial micro-Raman setup (HR LabRam inverse system, Jobin Yvon Horiba). The Raman scattering was excited by a frequency-doubled Nd: YAG laser at a wavelength of 532 nm with a laser power between 20 and 200 μW incident on the sample. The laser beam was focused on the sample by means of a Leica PLFluotar × 100/0.75 microscope objective down to a spot diameter of approximately 0.7 μm. The dispersive spectrometer has an entrance slit of 100 μm, a focal length of 800 mm and is equipped with a grating of 300 lines/mm. The Raman scattered light was detected by a Peltier-cooled charge coupled device (CCD) detector. The integration time for one Raman spectrum ranged from 60 to 240 s. The low values for the laser power and the relatively short acquisition times were chosen to avoid any possible changes in the samples.

Results and Discussion

The five different ironstone types can be grouped into three ironstone groups based on optical microscopic evaluation, revealing their mineralogical composition:

1. The black manganiferous mud and fossiliferous ironstone types
2. The yellowish-brown microbially-mediated ironstone types (stromatolitic and nummulitic–ooidal–oncoidal ironstone types).
3. The dark brown lateritic iron ore.

The investigated stromatolitic and nummulitic–ooidal–oncoidal ironstone samples of the present study indicate that the main iron mineral detected by means of Raman spectroscopy in these two types is goethite (Fig. 1). Goethite is an iron oxyhydroxide

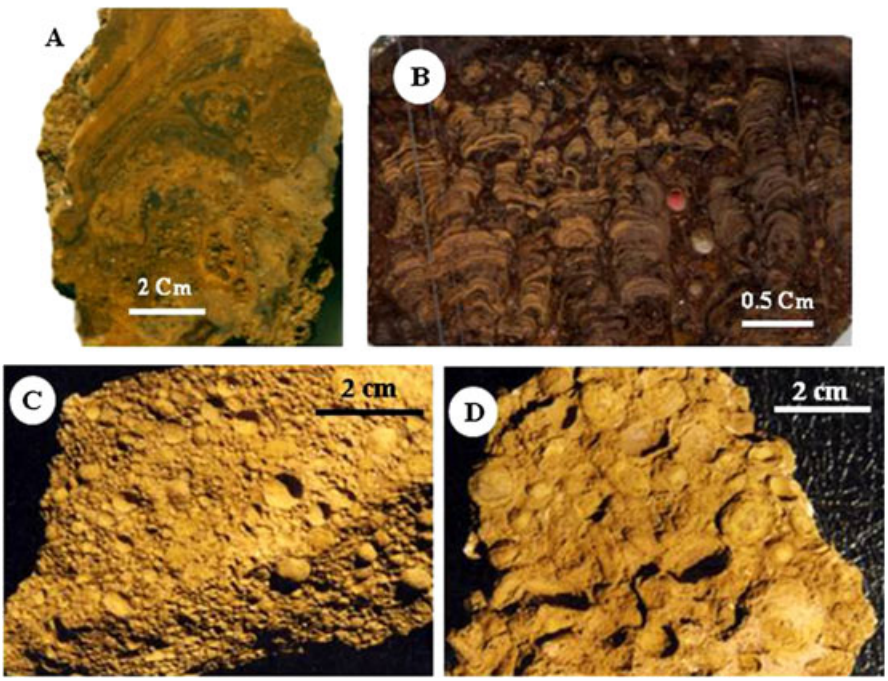

Figure 1. (A) A hand sample shows the even to wavy stromatolitic laminations of the stratiform stromatolites; (B) A hand sample shows stromatolite columns; (C) A hand sample of the nummulitic–ooidal–oncoidal ironstone type shows ferriferous ooids and few oncoids; and (D) A hand sample of the ferriferous oncoids.

Journal of RAMAN SPECTROSCOPY

(α-FeOOH), which presents a *Pbnm* space group symmetry. The Raman bands assigned to α-FeOOH are located at 291, 390, 471, 543, 681 and 990 cm^{-1} (Fig. 2(f)).[19] In addition to goethite, hematite was also detected in the investigated rock samples as the next dominant iron mineral. In contrast to the stromatolitic and nummulitic–ooidal–oncoidal ironstone samples, hematite was the main iron mineral in the manganiferous mud and fossiliferous ironstone samples. Hematite, α-Fe_2O_3, has a structural type of corundum, the space group is $R\bar{3}c$ with two formula unit per unit cell. Raman signals at 288, 406, 496, 607 and 1314 cm^{-1} (Fig. 2(g)) are characteristic of this mineral.[34] Because goethite and hematite exhibit larger Raman cross-sections than the manganese-containing minerals and are present in high concentration within the samples, the most intense bands of these two iron oxides are often detected together with signals from the other manganese minerals. For example, in Fig. 2 the spectra assigned to romanechite ($(Ba,H_2O)_2(Mn^{4+},Mn^{3+})_5O_{10}$), todorokite ($(Na,Ca,K)_2(Mn^{4+},Mn^{3+})_6O_{12}\cdot 3–4.5(H_2O)$), manjiroite ($(Na,K)(Mn^{4+},Mn^{2+})_8O_{16}\cdot n(H_2O)$), hollandite ($Ba(Mn^{2+}Mn^{4+})_8O_{16}$) and pyrolusite ($MnO_2$) show low wavenumber bands because of the presence of iron oxides/oxyhydroxides. However, the main Raman bands of various manganese oxides are located in the wavenumber region 500–650 cm^{-1}, thus away from the wavenumber area where goethite and hematite exhibit the strongest Raman signals (200–400 cm^{-1}). Therefore, the identification of Mn-containing minerals is not hindered by the presence of various iron oxides and/or oxyhydroxides.

Figure 2(a) shows the Raman spectrum of pyrolusite, with bands at 332, 534, 660 and 748 cm^{-1}. The Raman signals at 290, 407 and 1314 cm^{-1} are characteristic for hematite, which can be found in large amounts in the sample. The very weak Raman signals of pyrolusite at lower wavenumbers reported by other authors were probably completely overlapped by the intense Raman signals of the iron oxide.[20] The hollandite spectrum presented in Fig. 2(b) is dominated by the peak at 582 cm^{-1} with a shoulder at 624 cm^{-1}. The manjiroite and todorokite Raman spectra are presented in Figs 2(c) and (d), respectively. The main band of the two minerals is located at 643 and 645 cm^{-1}, respectively. The major difference between the two spectra is the appearance of a shoulder at 595 cm^{-1} in the spectrum of todorokite. The Raman bands appearing at lower wavenumbers can be assigned as well to iron oxides/oxyhydroxides. Figure 2(e) depicts the Raman spectrum of romanechite which is dominated by two partially overlapping bands at 583 and 644 cm^{-1}. The assignment of the Raman bands of the Mn-containing minerals are in concordance with previously reported investigations.[20]

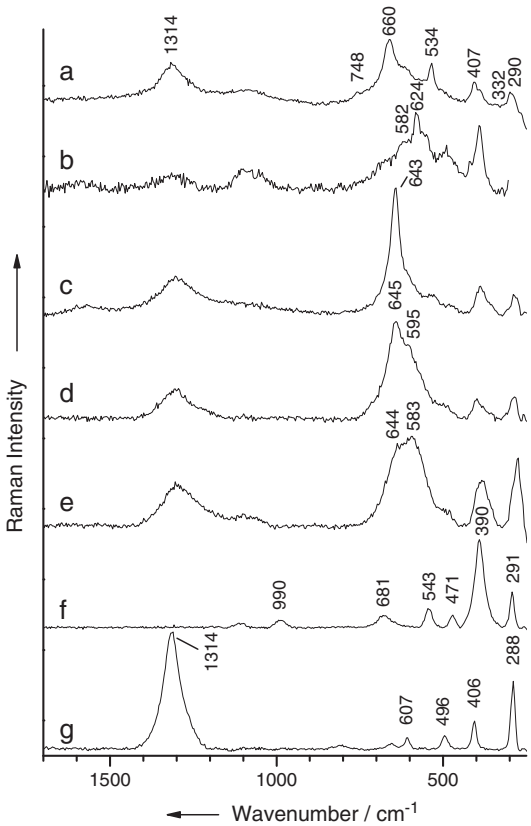

Figure 2. Raman spectra of various manganese and iron minerals recorded from various parts of the investigated samples: a – pyrolusite; b – hollandite; c – manjiroite; d – todorokite; e – romanechite; f – goethite; f – hematite.

The samples under study contain a large variety of manganese oxides. In the investigated samples, Mn forms oxides alone (pyrolusite) or in combination with barium (romanechite and hollandite) or sodium (manjiroite and todorokite). Although the provenience of the rock samples is from an arid zone (Western Dessert, Egypt), minerals which incorporate water inside the cell structure were also detected (todorokite and manjiroite). Interestingly, in all the Mn-containing minerals, Mn in the 4+ oxidation state was present. This suggests that the formation of the rocks took place in an acidic environment.

Pyrolusite, hollandite and romanechite were the most abundant Mn-containing minerals detected in all three types of the investigated samples. The other manganese minerals were detected only in the mud and fossiliferous ironstone samples.

Besides Mn in various forms, the rock samples also contained calcium-containing minerals. Figure 3 shows Raman spectra obtained from different calcium-containing minerals. In combination with phosphate, calcium was detected in the investigated materials as apatite in the lateritic and microbially-mediated ironstones. The Raman spectrum is dominated by the stretching vibration of the P–O bond at 960 cm^{-1} (Fig. 3(a)). Other Raman bands assigned to apatite can be found at 585 and 1076 cm^{-1}. As with the Mn-containing minerals, the low wavenumber Raman bands are attributed to the presence of iron oxides. Two different calcium carbonates were detected in the samples. Calcite ($CaCO_3$) (Fig. 3(b)) and dolomite ($CaMg(CO_3)_2$) (Fig. 3(e)) show intense Raman bands at 1086 and 1098 cm^{-1}, respectively, which can be assigned to the symmetric stretching vibrations of the C–O bonds in CO_3 tetrahedra.[35] Aside from the Raman band at 1086 cm^{-1}, two other bands are assigned to calcite: the bands at 282 and 712 cm^{-1}. Because very small amounts of dolomite are present in the microbially-mediated ironstone samples, only the most intense Raman band of this mineral appears in the Raman spectra of the investigated rocks. The remaining Raman bands in the spectrum shown in Fig. 3(e) belong to goethite (Fig. 2(f)). Figure 3(c) displays the Raman spectrum of anhydrite. The Raman bands which are attributed to this calcium sulfate mineral are found at 414, 497, 605, 624, 672, 1013, 1108, 1126 and 1158 cm^{-1}. The most intense Raman signal at 1013 cm^{-1} can be assigned to the S–O symmetric stretching vibration. In the case of gypsum ($CaSO_4\cdot 2H_2O$) (Fig. 3(d)), the S–O band is shifted to lower wavenumbers at 1009 cm^{-1}. The Raman signals at 416, 624, 672 and 1135 cm^{-1} are also assigned to this mineral. The remaining Raman bands shown in Fig. 3(d) belong to goethite. The last spectrum plotted in Fig. 3(f) is attributed to rapidcreekite,

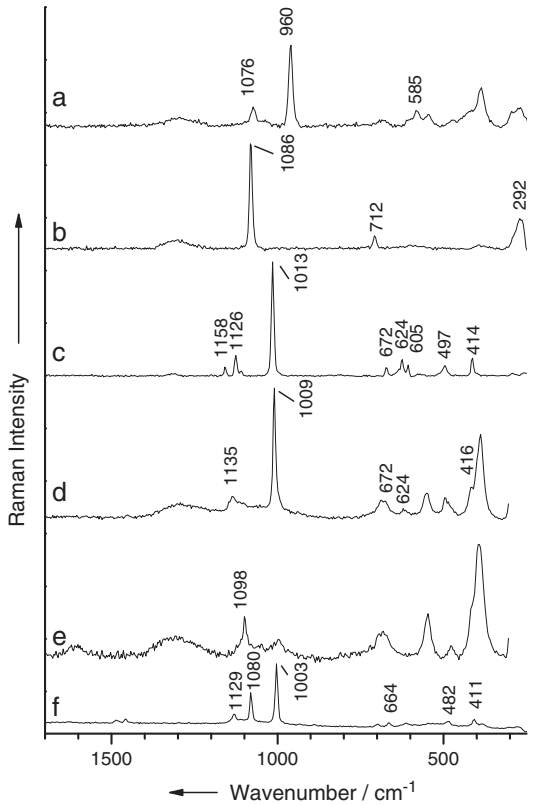

Figure 3. Raman spectra of different minerals containing calcium: a – apatite; b – calcite; c – anhydrite; d – gypsum; e – dolomite; f – rapidcreekite.

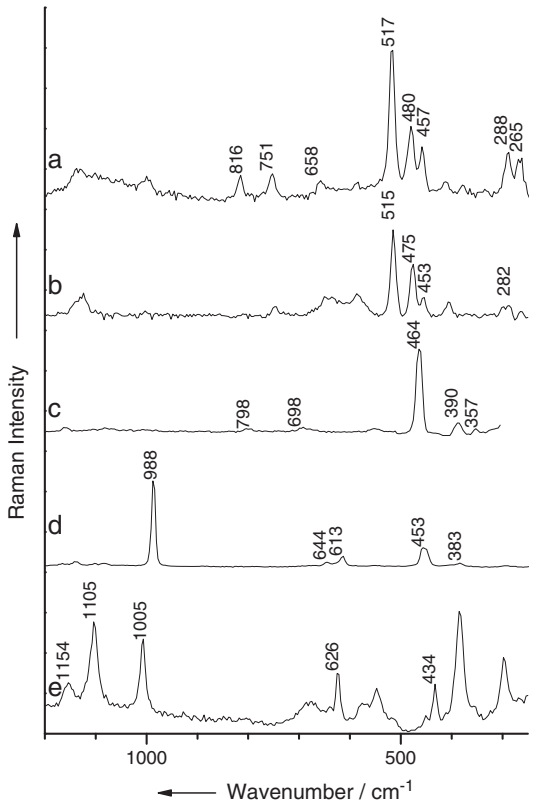

Figure 4. Various minerals detected by means of Raman spectroscopy: a – microcline; b – orthoclase; c – quartz; d – baryte; e – jarosite.

$Ca_2SO_4CO_3{\cdot}4H_2O$. The C–O symmetric stretching vibration band is located at 1003 cm^{-1}, whereas the S–O symmetric stretching vibration band shows up at 1080 cm^{-1}. The Raman bands at 382, 411, 486, 611, 664 and 1129 cm^{-1} are typical for rapidcreekite.[36]

Figure 4 shows the Raman spectra of other minerals detected in the investigated rock samples. The Raman bands at 265, 288, 457, 480, 517, 658, 751 and 816 cm^{-1} are assigned to microcline ($KAlSi_3O_8$) (Fig. 4(a)). Microcline and orthoclase are polymorphs, microcline having a triclinic structure while orthoclase a monoclinic one. The main difference between the Raman spectra of the two minerals represents the triplet bands at 656, 751 and 816 cm^{-1}, which are much more intense in the case of microcline compared to orthoclase[37] (Fig. 4 (b)). Another difference between the two spectra is the number of Raman bands exhibited by the two minerals. Makreski *et al.* showed that the spectra of the more ordered feldspars are richer in bands than the spectra of feldspars with a lower structural symmetry.[38] Another mineral detected in the samples was quartz (SiO_2) (Fig. 4(c)) with its main Raman band, the Si–O stretching vibration, leading to the very intense Raman signal at 464 cm^{-1}. Additionally, bands at 357, 390, 698 and 798 cm^{-1} are also attributed to quartz. Figure 4(d) presents the Raman spectrum of barite ($BaSO_4$) with its characteristic Raman signals at 383, 453, 613, 644 and 988 cm^{-1}.[36]

A further indication of an acidic pH of the environment during mineral formation (*vide supra*) can be seen in the detection of jarosite ($KFe(SO_4)_2(OH)_6$) and anglesite ($PbSO_4$). Jarosite and anglesite can only be formed in an acidic pH in arid climates via oxidation of iron and lead sulfides, respectively. Raman signals at 434, 626, 1005, 1105 and 1154 cm^{-1} (Fig. 4(e)) are assigned to these minerals.[39,40]

Besides inorganic minerals, Raman signals for organic matter can also be found in the ironstone spectra. Figure 5(a) displays the Raman spectrum of a carotenoid with its three characteristic Raman bands at 1000, 1150 and 1515 cm^{-1}. The position and the sharpness of the Raman bands suggest that the organic compounds were very well preserved in the rocks.[41] The size of the spots where carotenoids were detected has a diameter of a few micrometers. A large variety of organisms can produce different types of pigments (chromophores); therefore, the carotenoids can represent a biomarker for bacteria, fungi and/or algae. The presence of carotenoids in the samples demonstrates that the formation of the second group of ironstone samples was biologically mediated.

Much more difficult to interpret are the Raman spectra (b) and (c) of Fig. 5. Spectrum (b) can be assigned to a proteinaceous matter[6] while spectrum (c) presents the main bands of a lipid compound.[42] A possible explanation of the origin of those materials can be that they are from marine organisms such as mollusks, echinoderms and nummulites, and also microbial organisms.

Cellulose was also detected in the oncoids (Fig. 5(d)). The cellulose particles have usual rod shapes and are a few tens of micrometers in length. In the supporting information, a Raman image of such a particle is presented. However, no lignin was detected in the samples. Therefore, the absence of lignin might suggest that the cellulose originated from algae, fungi or bacteria and not from plants.[43]

Raman measurements performed on freshly broken samples also show bands from organic matter and thus prove that organic matter is really a component of the ironstones and not just an artifact.

Journal of RAMAN SPECTROSCOPY

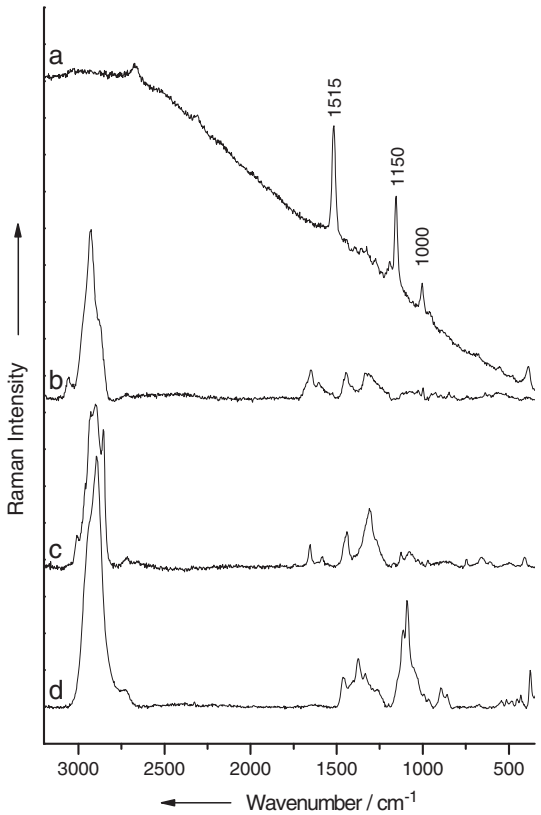

Figure 5. Organic materials detected by means of micro-Raman spectroscopy: a – carotenoid; b – proteinaceous compound; c – lipid compound; d – cellulose.

The main iron-containing minerals detected in the mud and fossiliferous ironstones were hematite and goethite, whereas the main manganese minerals were todorokite, birnessite, manjiroite, aurorite, pyrolusite, hollandite and romanechite. The detrital (transported) minerals such as quartz, orthoclase, microcline, rutile and late-cementing minerals such as barite, calcite and anhydrite were also identified in the samples.

The mineralogical composition of the stromatolitic laminae and the cortical laminae of the ferriferous oncoids and ooids consisted of ferric iron oxyhydroxides (goethite) mixed with ferric iron hydroxysulfate (jarosite), whereas the ferric iron oxide (hematite) was mainly detected as cement surrounding the ooids and oncoids. Other mineral groups were also identified, including phosphates (apatite), carbonates (calcite and dolomite), sulfates (gypsum, anhydrite and barite), manganese minerals (pyrolusite, hollandite and romanechite) and silicates (quartz). In addition, various preserved organic materials inside the stromatolitic laminae and the cortical laminae of the ferriferous oncoids and ooids were detected by means of Raman spectroscopy.

The lateritic ironstones were mainly made up of ferric iron oxides and oxyhydroxides (hematite and goethite), ferric iron hydroxysulfate (jarosite) and manganese minerals (pyrolusite, hollandite and romanechite). Other mineral groups such as authigenic phosphates (apatite), late cement carbonate (calcite) and sulfates (gypsum, anhydrite, rapidcreekite and barite), and detrital silicates (quartz) were also identified.

Goethite, hematite, quartz and calcite are common minerals in all ironstone types. They were also identified with the optical microscope and the conventional X-ray diffraction technique. On the other hand, the black color of the manganese minerals, yellowish-brown color of goethite and jarosite and the colorless minerals such as gypsum, anhydrite, rapidcreekite, barite, anglesite, nitratine, dolomite and apatite did not allow their identification under the optical microscope. Moreover, the small crystal sizes and/or inhomogeneous distribution (cavity and fracture-filling phases) of such minerals did not allow the collection of enough materials for the X-ray diffraction (XRD) analyses.

Information about the diagenetic modifications in the studied materials was obtained by combining Raman spectroscopy with optical and scanning electron microscopy (SEM). The original iron oxyhydroxide precipitates were amorphous or nanocrystalline that were transformed by recrystallization into goethite and then by dehydration to hematite.[44] The organic matter degradation can release substantial amounts of phosphorus into pore waters. The supersaturation of the pore waters with phosphorus resulted in the development of diagenetic apatite crystals.[45] Moreover, diagenetic clay minerals, such as kaolinite and illite develop at the expense of detrital feldspar crystals, such as orthoclase and microcline. The clay minerals were identified by XRD, SEM and energy-dispersive X-ray spectroscopy (EDX).[2]

Conclusions

The present study illustrates the application of micro-Raman spectroscopy for the solution of a geological problem concerning the origin of the Egyptian Middle Eocene ironstones. Information about the complex environmental conditions prevailing during and after the ironstone formation can be gained by analyzing all the organic and inorganic mineral phases of these ironstones.

The application of micro-Raman spectroscopy provides important and precise information concerning the identification of iron oxides and oxyhydroxide minerals (goethite and hematite), manganese minerals (todorokite, birnessite, pyrolusite, hollandite, romanechite, aurorite and manjiroite), sulfates (jarosite, gypsum, anhydrite, rapidcreekite, barite and anglesite), nitrates (nitratine), carbonates (calcite and dolomite), silicates (quartz, orthoclase, microcline), heavy minerals (rutile) and phosphate (apatite) minerals. Attempts to identify such mineral species with optical microscopy and the conventional X-ray diffraction technique were difficult or impossible.

However, we were not able to identify clay minerals by means of Raman spectroscopy.

The detection of romanechite, anglesite and jarosite is a good indication of low pH acidic conditions during the formation of these minerals. The presence of sulfate, nitrate and carbonate minerals (calcite, gypsum, anhydrite, rapidcreekite, nitratine and halite), which occurs as cavity filling, indicate recent to subrecent mineralogical and chemical alterations typical for the young weathering crusts in the arid zone of NE Africa's desert. Furthermore, the detection of organic materials and apatite within the ferriferous ooids and oncoids provides a clear evidence of the biological mediation involved in the process of mineral formation.

Supporting information

Supporting information may be found in the online version of this article.

Acknowledgements

We highly acknowledge the financial support from the Deutsche Forschungsgemeinschaft (Graduate School 1257 'Alteration and

element mobility at the microbe–mineral interface'). In addition, this work was supported by the German Academic Exchange Service (DAAD), and the Thüringische Ministerium für Bildung, Wissenschaft und Kultur (TMBWK) under the project code "MikroPlex" PE113–1, through two years Sandwich program (Channel system) grant of Walid Salama.

References

[1] M. M. El Aref, A. A. Mesaed, M. A. Khalil, W. S. Salama, *Egypt. J. Geol.* **2006a**, *50*, 29.
[2] W. S. Salama, Geological and Mineralogical Studies on the Microbially-mediated Ironstone Facies, El Baahriya Depression, Western Desert, Egypt, Ph. D.Thesis, Faculty of Science, Cairo University, **2010**.
[3] N. J. Shackleton, *Palaeogeogr., Palaeoclimatol., Palaeoecol.* **1986**, *57*, 91.
[4] D. R. Prothero, W. A. Berggren, P. R. Bjork, *Geol. Soc. Am. News Inform.* **1990**, *12*, 74.
[5] M. M. El Aref, A. A. Mesaed, M. A. Khalil, W. S. Salama, *Egypt. J. Geol.* **2006b**, *50*, 59.
[6] H. G. M. Edwards, *Analyst* **2004**, *129*, 870.
[7] A. Hernanz, J. M. Gavira-Vallejo, J. F. Ruiz-López, H. G. M. Edwards, *J. Raman Spectrosc.* **2008**, *39*, 972.
[8] M. Castriota, V. Cosco, T. Barone, G. D. Santo, P. Carafa, E. Cazzanelli, *J. Raman Spectrosc.* **2008**, *39*, 295.
[9] M. Christensen, M. Frosch, P. Jensen, U. Schnell, Y. Shashoua, O. F. Nielsen, *J. Raman Spectrosc.* **2006**, *37*, 1171.
[10] P. Vandenabeele, B. Wehling, L. Moens, H. Edwards, M. De Reu, G. Van Hooydonk, *Anal. Chim. Acta* **2000**, *407*, 261.
[11] F. Ospitali, D. C. Smith, M. Lorblanchet, *J. Raman Spectrosc.* **2006**, *37*, 1063.
[12] H. G. M. Edwards, D. W. Farwell, *Spectrochim. Acta, Part A* **1995**, *51*, 2073.
[13] P. Vargas Jentzsch, B. Kampe, P. Rösch, J. Popp, *J. Phys. Chem. A* **2011**, *115*, 5540.
[14] S. Cînta Pînzaru, B. P. Onac, *Vib. Spectrosc.* **2009**, *49*, 97.
[15] J. Jehlicka, H. G. M. Edwards, *Org. Geochem.* **2008**, *39*, 371.
[16] S. K. Sharma, P. G. Lucey, M. Ghosh, H. W. Hubble, K. A. Horton, *Spectrochim. Acta, Part A* **2003**, *59*, 2391.
[17] R. L. Frost, R.-A. Wills, M. L. Weier, W. Martens, S. Mills, *Spectrochim. Acta, Part A* **2006**, *63*, 1.
[18] M.-C. Bernard, A. H.-L. Goff, B. V. Thi, S. C. de Torresi, *J. Electrochem. Soc.* **1993**, *140*, 3065.
[19] D. L. A. Faria, S. V. Silva, M. T. Oliveira, *J. Raman Spectrosc.* **1997**, *28*, 873.
[20] C. M. Julien, M. Massot, C. Poinsignon, *Spectrochim. Acta, Part A* **2004**, *60*, 689.
[21] I. Martínez-Arkarazo, M. Angulo, O. Zuloaga, A. Usobiaga, J. M. Madariaga, *Spectrochim. Acta, Part A* **2007**, *68*, 1058.
[22] E. A. Stefaniak, A. Worobiec, S. Potgieter-Vermaak, A. Alsecz, S. Török, R. Van Grieken, *Spectrochim. Acta, Part B* **2006**, *61*, 824.
[23] T. Dörfer, W. Schumacher, N. Tarcea, M. Schmitt, J. Popp, *J. Raman Spectrosc.* **2010**, *41*, 684.
[24] R. Petry, R. Mastalerz, S. Zahn, T. G. Mayerhöfer, G. Völksch, L. Viereck-Götte, B. Kreher-Hartmann, L. Holz, M. Lankers, J. Popp, *Chemphyschem* **2006**, *7*, 414.
[25] V. Ciobotă, E.-M. Burkhardt, W. Schumacher, P. Rösch, K. Küsel, J. Popp, *Anal. Bioanal. Chem.* **2010**, *397*, 2929.
[26] F. Rull, J. Martinez-Frias, J. A. Rodríguez-Losada, *J. Raman Spectrosc.* **2007**, *38*, 239.
[27] W. Schumacher, M. Kühnert, P. Rösch, J. Popp, *J. Raman Spectrosc.* **2011**, *42*, 383.
[28] N. Tarcea, M. Harz, P. Rösch, T. Frosch, M. Schmitt, H. Thiele, R. Hochleitner, J. Popp, *Spectrochim. Acta, Part A* **2007**, *68*, 1029.
[29] T. Frosch, N. Tarcea, M. Schmitt, H. Thiele, F. Langenhorst, J. Popp, *Anal. Chem.* **2007**, *79*, 1101.
[30] R. Hochleitner, N. Tarcea, G. Simon, W. Kiefer, J. Popp, *J. Raman Spectrosc.* **2004**, *35*, 515.
[31] V. Klein, J. Popp, N. Tarcea, M. Schmitt, W. Kiefer, S. Hofer, T. Stuffler, M. Hilchenbach, D. Doyle, M. Dieckmann, *J. Raman Spectrosc.* **2004**, *35*, 433.
[32] S. E. Jorge Villar, H. G. M. Edwards, L. G. Benning, *Icarus* **2006**, *184*, 158.
[33] J. Jehlicka, H. G. M. Edwards, P. Vítek, *Planet. Space Sci.* **2009a**, *57*, 606.
[34] G. N. Kustova, E. B. Burgina, V. A. Sadykov, S. G. Poryvaev, *Phys. Chem. Miner.* **1992**, *18*, 379.
[35] Z. Tomić, P. Makreski, B. Gajić, *J. Raman Spectrosc.* **2010**, *41*, 582.
[36] J. Jehlicka, P. Vítek, H. G. M. Edwards, M. Heagraves, T. Capoun, *Spectrochim. Acta, Part A* **2009b**, *73*, 410.
[37] J. Yang, G. Godard, D. C. Smith, *Eur. J. Mineral.* **1998**, *10*, 969.
[38] P. Makreski, G. Jovanovski, B. Kaitner, *J. Molec. Struct.* **2009**, *924–926*, 413.
[39] H. G. M. Edwards, P. Vandenabeele, S. E. Jorge-Villar, E. A. Carter, F. R. Perez, M. D. Hargreaves, *Spectrochim. Acta, Part A* **2007**, *68*, 1133.
[40] P. Makreski, G. Jovanovski, S. Dimitrovska, *Vib. Spectros.* **2005**, *39*, 229.
[41] C. P. Marshall, A. Olcott Marshall, *Phil. Trans. R. Soc. A* **2010**, *368*, 3137.
[42] M. Harz, M. Kiehntopf, S. Stöckel, P. Rösch, T. Deufel, J. Popp, *Analyst* **2008**, *133*, 1416.
[43] M. Strømme, A. Mihranyan, R. Ek, *Mater. Lett.* **2002**, *57*, 569.
[44] H. Harder, in Geological Society Special Publications, *vol. 46* (Eds.: T. P. Young, W. E. G. Taylor), Geological Society of London, London, **1989**, pp. 9.
[45] N. Tribovillard, T. J. Algeo, T. Lyons, A. Riboulleau, *Chem. Geol.* **2006**, *232*, 12.